2020 IEEE International Conference on Power Electronics, Drives and Energy Systems (PEDES) | 978-1-7281-5672-9/20/$31.00 ©2020 IEEE | DOI: 10.1109/PEDES49360.2020.9379849

Analysis of magnetic materials and the design of EI-core arm inductor for MV-AFE MMC application using Multi-objective optimization

Rounak Siddaiah, Robert M. Cuzner
Center for Sustainable Electric Energy Systems
University of Wisconsin-Milwaukee
Milwaukee, WI, USA
frounak@uwm.edu and cuzner@uwm.edu

***Abstract*—The Modular Multi-Level Converter (MMC) is a popular topology for HVDC or MVDC microgrids which require 6 (2 per phase) arm inductors for each system which are significant in size. Therefore characterizing different magnetic materials for a MV inductor design process is very important for power density. Many variables must be analyzed before expensive MV inductors are manufactured. Inductor design is a multi-objective optimization problem that is tackled by using an evolutionary algorithm to solve this is shown in this paper. Loss, Mass, and volume are optimized using a genetic algorithm for a 2mH, 297 A(rms) MMC arm inductor with an E-I core structure.**

***Index Terms*—MMC, Multi-objective optimization, EI-core, Anhysteric characterization, Magnetic materials.**

I. Introduction

Modular multi-level converter(MMC) has been one of the most researched multilevel topology because of its numerous advantages of stacking sub-modules in series, operating at high voltages, etc. [1]–[3]. Selection of passive components depends on the application, the power requirement level and minimization of circulating current [4], [5]. One of the most unique feature of the Full bridge MMC is that it provides DC fault current blocking capability, which requires the arm inductor to be of significant size [6]–[8]. Consideration of all the parameters associated with the magnetic design to achieve an optimal design concerning power density should be of paramount concern, especially for space-constrained applications, such as Medium Voltage DC (MVDC) distribution in naval vessels [9], where the MMC is considered of high value because of its fault management capability [10]. This work supports an ongoing effort to understand how the choice of Power Electronic Converter (PEC) topologies impacts the approach to MVDC shipboard electrification. Optimal design of the PEC and sub-components making up a given PEC topology is critical to informing of electrical architectural decisions [11]–[14]. The MMC topology is shown in Fig. 1. This paper focuses on the arm inductor specifically and the use of emerging magnetic material technologies suitable for high voltage and high frequency application. Anhysteric characterization of these new ferromagnetic or ferrimagnetic materials is very useful to optimal design of these magnetic components such as inductors and high frequency transformer, as explained in section III. [15].

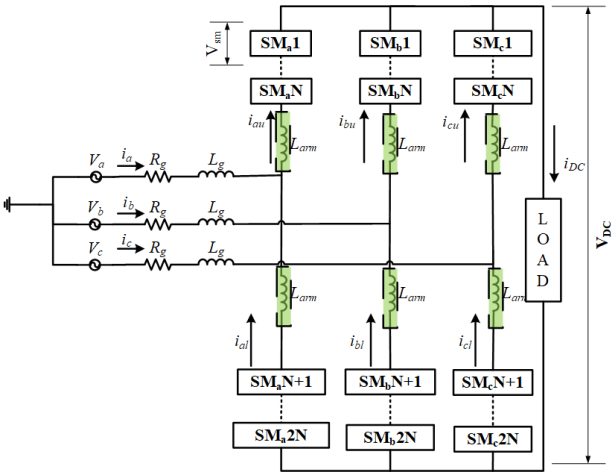

Fig. 1. MMC Circuit Architecture

II. Magnetic material considered

The magnetic parameters of soft magnetic materials that are being considered as shown in Table I are generated from the experimental setup described in [15], [16]. The datasheets for these magnetic materials are listed in [17], [18].

- FINEMET® isa nanocrystalline material, which is a soft magnetic material with a chemical composition of $Fe_{73.5}Nb_3Si_{15.5}B_7Cu_1$.
- FT3L is also a nanocrystalline material which is suitable for medium frequency transformers and high-power applications.

This material is based upon work supported by the Office of Naval Research (ONR), grants N00014-20-1-2667 and N00014-18-1-2622, National Science Foundation (NSF) grant 1650470 and industry supported research support through the Midwest Energy Research Consortium (M-WERC) of Milwaukee, WI

- MK-Prime-NC-0001-3- is a wide tape-wound core, manufactured with FINEMET® iron-based metal amorphous nanocomposite.
- METGLAS® 2605-SA1 is an amorphous tape wound core, manufactured with iron-based 2605-SA1 amorphous foil.
- GRMAG-1-12-360 is a tape-wound core, manufactured with a custom iron-based metal amorphous nanocomposite.
- 3% (Grain-Oriented) and 6.5% (Non-Grain-Oriented) Silicon Steel have a chemical composition of $Fe_{94.2}Si_{5.8}$ and $Fe_{87.9}Si_{12.1}$, respectively, and are soft magnetic materials best used in low frequency power transformers and inductors.
- EPCOS N87 is an oxide made from Fe (iron), Mn (manganese), and Zn (zinc), which are commonly referred to as manganese zinc ferrites.

In this paper, the focus is to use the magnetic materials mentioned in Table I. In our previous work, we have used the list of materials mentioned below

$$CoreMaterial = \left\| \begin{array}{cc} \textbf{Silicon steel} & \textbf{Ferrite} \\ M19 & MN8CX \\ M36 & MN60LL \\ M43 & MN67 \\ M47 & MN80C \\ Hyperco50 & 3C90 \end{array} \right\| \quad (1)$$

which have been characterized and are well established using Genetic algorithm as part GOSET [16].

III. Anhysteric Characterization Procedure

Anhysteric characterization via the anhysteretic magnetization curve is a useful approach to modeling of magnetic material within a magnetic component optimization process. The fundamental concept and the modeling process is defined by and explained in [15], [18]. The anhysteretic relationship between flux density B , field intensity H , and magnetization M is

$$B = \mu_0 H + M \quad (2)$$

where $\mu_0$is the permeability of free space. μ can also be represented in-terms of B and H as $B = \mu_B(B)M$ and $B = \mu_H(H)M$ respectively. The Magnetization is represented as

$$M(H) = sgn(H) \sum_{k=1}^{K} \frac{\mathrm{m_k}|\mathrm{H}/\mathrm{h_k}|}{1 + |\mathrm{H}/\mathrm{h_k}|^{\mathrm{n_k}}} \quad (3)$$

where $sgn(H)$ denotes the sign function, $\mathrm{m_k}$, $\mathrm{n_k}$, and $\mathrm{h_k}$ are constants, and K is the number of terms used. The variable K refers to the four coefficients listed in the Table I. The corresponding anhysteric B-H curves of the first quadrant, for the materials under consideration, are shown in Fig. 2, where

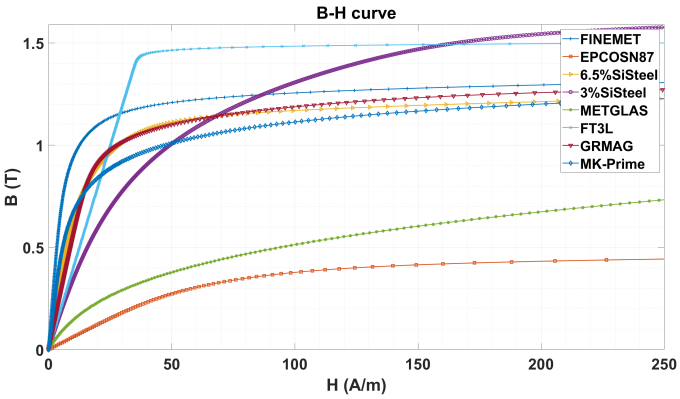

Fig. 2. Anhysteric B-H curve of the first quadrant

H is limited to 250A/m. Also for permeability modeling, the $\mu_H(H)$ and $\mu_B(B)$is defined as

$$\mu_H(H) = \mu_0 + sgn(H) \sum_{k=1}^{K} \frac{\mathrm{m_k}}{\mathrm{h_k}} \frac{1}{1 + |\mathrm{H}/\mathrm{h_k}|^{\mathrm{n_k}}} \quad (4)$$

$$\frac{\mathrm{d}\mu_B(B)}{\mathrm{d}B} = \frac{\mu_0}{(\mathrm{r(B)} - 1)^2} \frac{\mathrm{d}g(B)}{\mathrm{d}B} \quad (5)$$

where

$$\frac{\mathrm{d}g(B)}{\mathrm{d}B} = sgn(B) \sum_{k=1}^{K} \frac{\eta_\mathrm{k}}{\theta_\mathrm{k} + \mathrm{e}^{-\beta_\mathrm{k}|\mathrm{B}|}} \quad (6)$$

which is also represented as

$$g(B) = \sum_{k=1}^{K} \alpha_k B + \delta_k \ln(\epsilon_k + \zeta_k e^{-\beta_k |B|}) \quad (7)$$

where α_k, β_k and γ_k are defined by Table I and the remaining variables are defined by

$$\delta_k = \frac{\alpha_\mathrm{k}}{\beta_\mathrm{k}} \quad (8)$$

$$\epsilon_k = \frac{\mathrm{e}^{(-\beta_\mathrm{k}\gamma_\mathrm{k})}}{1 + \mathrm{e}^{(-\beta_\mathrm{k}\gamma_\mathrm{k})}} \quad (9)$$

$$\zeta_k = \frac{1}{1 + \mathrm{e}^{(-\beta_\mathrm{k}\gamma_\mathrm{k})}} \quad (10)$$

$$\eta_k = \alpha_k e^{(-\beta_k \gamma_k)} \quad (11)$$

$$\theta_k = e^{(-\beta_k \gamma_k)} \quad (12)$$

IV. System Modeling and Formulation of Optimization Problem

Optimization of a Medium voltage and High current inductor is a crucial step in developing scaling laws and Metamodels for range of applications mentioned above [16], [19]–[21]. Inductor optimization is dependent on many objectives, this study is limited to Loss, Mass and Volume of the EI-core inductor, any other core shape can be considered and a comparative study can be presented. However, for the sake

978-1-7281-5672-9/20/$31.00 ©2020 IEEE

TABLE I
MATERIAL PARAMETERS

Material μ_r	**Parameter (Pa)**	**1**	**2**	**3**	**4**	**Pa**	**1**	**2**	**3**	**4**
FINEMET	m_k	1.4543	-0.78747	0.30582	-0.1001	α_k	0.60159	0.037315	0.037134	0.005472
122403.68	h_k	1.66902	4.53941	16.3984	2.21434	β_k	49.09419	6.051651	342.7715	26.75667
	n_k	1	1.3918	1.9193	2.4723	γ_k	1.4323	2.1063	1.4132	1.3
EPCOSN87	m_k	0.61604	-0.11219	0.18713	0.32051	α_k	0.77671	0.10936	0.0020333	0.0020331
4969.053	h_k	176.0002	62.83682	234.2771	85.26742	β_k	91.3632	44.8969	2.33887	16.8801
	n_k	1	1.1415	2.1936	2.4034	γ_k	0.55132	0.48894	2.8476	0.35151
6.5%SiSteel	m_k	1.6197	-0.068259	-0.82772	0.34521	α_k	0.59215	0.046468	0.002606	0.0023773
62847.667	h_k	14.7265	3.67467	76.743	27.7231	β_k	20.6209	96.0792	42.3268	4.65204
	n_k	1	2.85	1.283	1.2574	γ_k	1.5593	1.4973	1.172	1.6916
3%SiSteel	m_k	1.7533	-0.090621	0.19404	0.19157	α_k	0.50799	0.031	0.001	0.001
30192.4844	h_k	44.52358	10.92945	252.4857	33.44442	β_k	98.3104	27.1445	3.12127	2.54436
	n_k	1	1.5246	3.8879	2.2249	γ_k	1.7509	1.6929	10	1.9774
METGLAS	m_k	1.4235	0.15032	-0.19397	-0.26992	α_k	0.62315	0.074964	0.0013134	0.0013134
16083.8541	h_k	131.7483	25.37762	220.6462	533.6291	β_k	65.8063	17.8022	2.02023	4.54498
	n_k	1	2.248	2.8643	3.2472	γ_k	1.4242	1.4102	10	0.4966
FT3L	m_k	1.5652	-0.035117	0.66116	0.35357	α_k	0.59017	0.59017	0.59017	0.59017
31643.8738	h_k	74.9869	34.098	63.1436	45.1082	β_k	78.047	78.047	78.047	78.047
	n_k	1	5	2.5427	4.8332	γ_k	1.5654	1.5654	1.5654	1.5654
GRMAG	m_k	1.3619	0.76562	-0.079225	0.18904	α_k	0.68789	0.032217	0.0043479	0.001
45064.6754	h_k	39.2995	24.8043	30.4181	28.1487	β_k	289.7214	66.28096	11.07119	4.2175
	n_k	1	1.6942	1.1	4.8707	γ_k	1.3251	1.3075	1.3222	2.1465
MK-Prime	m_k	1.4696	0.24151	-0.39216	-0.21175	α_k	0.5883	0.016237	0.016232	0.015558
82811.4222	h_k	9.59306	3.26685	96.8644	26.9715	β_k	63.9079	5.69495	14.1786	61.6236
	n_k	1	2.4164	1.5951	2.4178	γ_k	1.4585	1.7324	1.4044	1.3772

of in-depth analysis, the focus of this paper is only on EI core. For the interested reader, preliminary analysis for an UI core is performed in [22]. Here, a Multi-objective based evolutionary Genetic Algorithm (GA) is used to optimize the inductor. Although there other optimization algorithms could apply, the rationale behind the use of GA and the algorithm itself is justified in [22], [23]. Computationally efficient and accurate optimization of the inductor primarily depends on its magnetic loss modeling, as discussed in the section V. Inductor Design specifications for the 2mH, 297 A(rms) arm inductor are provided in Table II. In Table III the range of design space that are being considered for inductor design for multi-objective optimization is shown. The Complete GA design process for the EI-core inductor is illustrated in Fig. 3. For the GA to converge to a reasonable design, some constraints like maximum allowed mass, volume and loss should be specified. These are the three design objectives to optimize or maximize in a fitness function in GA.

$$(Fitnessfunction)f = \begin{Bmatrix} 1/Mass \\ 1/PowerLoss \\ 1/Volume \end{Bmatrix} \tag{13}$$

There are many evolutionary algorithmS available in the literature [24]. The proposed approach utilizes a fast and elitist multi-objective genetic algorithm, NSGA-II [25]m for formulation of fitness function. In order to test constraints, it is convenient to define the less than or the equal to, or greater than or equal to function [16]:

$$lte(x, x_{mx}) = \begin{Bmatrix} 1, & x \le x_{mx} \\ \frac{1}{1+\mathrm{x}-\mathrm{x_{mx}}}, & x > x_{mx} \end{Bmatrix} \tag{14}$$

$$gte(x, x_{mn}) = \begin{Bmatrix} 1, & x \ge x_{mn} \\ \frac{1}{1+\mathrm{x_{mn}}-\mathrm{x}}, & x < x_{mn} \end{Bmatrix} \tag{15}$$

The requirement may be to limit the volume, mass or loss, defined in GA as

$$C1 = lte(vol, vol_{mx}) \tag{16}$$

$$C2 = lte(Powerloss, Powerloss_{mx}) \tag{17}$$

$$C3 = lte(Mass, Mass_{mx}) \tag{18}$$

Maximizing the average of these normalized constraints should be achieved. The average of these constraints can be found by

$$\mathbb{C} = \frac{1}{\mathrm{C}} \sum_{i=1}^{C} C_i \tag{19}$$

978-1-7281-5672-9/20/$31.00 ©2020 IEEE

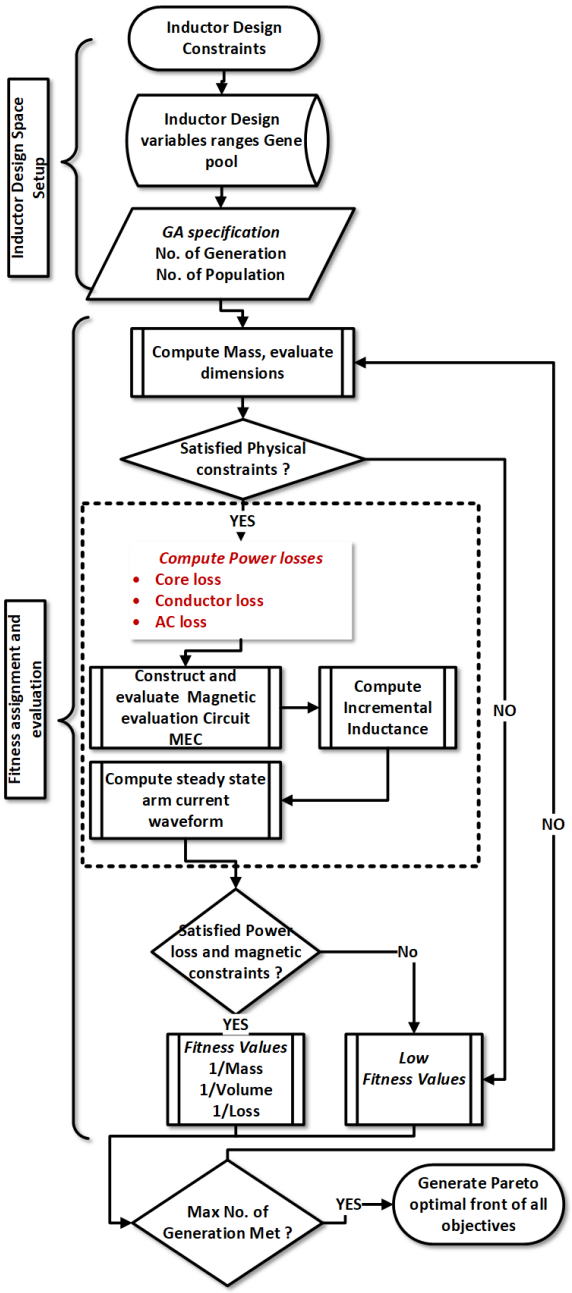

Fig. 3. Inductor Design Flowchart

The elements of the fitness function for this case study is defined by

$$f = \begin{Bmatrix} \varepsilon(\mathbb{C}-1), & \mathbb{C} < 1 \\ 1/Volume, & \mathbb{C} = 1 \\ 1/Mass, & \mathbb{C} = 1 \\ 1/Power - loss, & \mathbb{C} = 1 \end{Bmatrix} \quad (20)$$

where ε is a small positive value and it has no impact on the results of the generation. NSGA-II designs that do not meet all constraints will have negative fitness, whereas the others have positive fitness. The algorithm checks the fitness of the solution and determines to what degree of fitness should be given. If the fitness becomes to deteriorates the means the solution is moving further away from the ideal solution and performs elitist strategy and tournament selection to rank the solution. after which the successive solution might get better rank compared to the previous solution i.e. it may get more positive fitness.

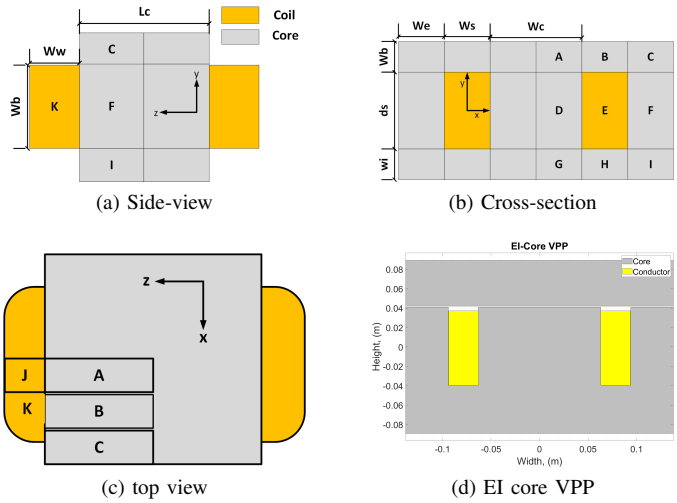

Fig. 4. EI-Core Inductor

A. Inductor design flowchart

In the previous section, setting up of fitness function was explained for a multi-objective optimization for a EI-core inductor. In this section, the overall process is looked into. This process is outlined as follows:

1) Inductor Design space setup: The inductor design space setup consists of inductor Design constraints, Inductor design variable range (gene pool) and GA specification (number of generation and number of population). Inductor Design specifications act as a boundary inside which the algorithm has to operate. The Inductor GA design space gives a range of options that the algorithm can use to come up with a feasible solution.

2) Fitness assignment and evaluation: Fitness assignment and evaluation is where the objectives of the optimization are established, and the values from one set of a population of the GA is assigned to the fitness function. In this case study, the design space used for optimization is defined by θ_{EI}. The design of a 2mH MMC arm inductor, the 297A E-I core is taken as a case study.

$$\theta_{EI} = \begin{bmatrix} g & l_c & w_{(i)} & r_{(j)} & a_c & N & Cw \end{bmatrix}^T \quad (21)$$

where g is the air gap of the E-I core inductor, L_c is the length of the indicator core, $w_{(i)}$ contains the different dimensions of the core, $r_{(j)}$ contains the aspect ratios of these cores, a_c is the cross-sectional area of the conductor, N is the number of turns and C_w is the slot width of the core. Also, in this case study, the conductor material is fixed as copper and the number of parallel conductors is constrained to 10 for AC losses.

978-1-7281-5672-9/20/$31.00 ©2020 IEEE

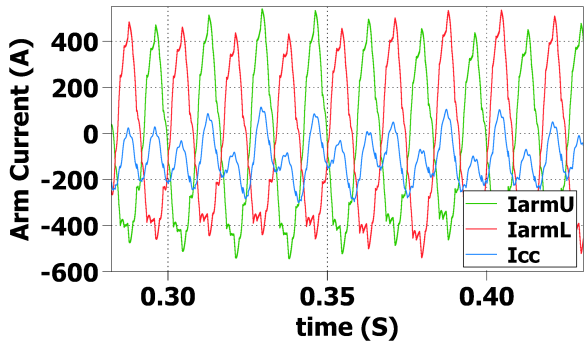

Fig. 5. Upper & Lower Arm currents and circulating currents Icc from the switching model simulation

From the randomized set of initial variables, mass and volume of the inductor can be computed very easily as the first step. For example, since these evaluations do not need the magnetic equivalence to be constructed and evaluated, the run time of the algorithm will be minimized and unnecessary designs will be eliminated before the inductance is calculated. If the mass and volume criteria are met, the next step would be to calculate magnetic loss and inductance. To perform this loss calculation a Magnetic equivalent circuit (MEC) should be constructed and incremental inductance should be calculated. The calculation of the AC loss must have a reasonable estimate for harmonic and high frequency characteristics (associated with power semiconductor switching) of the current waveform. This aspect of the design optimization is challenging because it requires analytical closed form equations that will reflect the dominant even harmonics of the fundamental frequency and the switching frequency fundamental and harmonic current amplitudes characteristic of the MMC arm inductor,as shown in Fig. 5 [23]. The resultant loss analysis is then checked to verify the satisfaction of the design criteria before moving forward to calculate the fitness values. The details of the loss calculation are explained in detail in section V.

3) Stopping criteria: The fitness is evaluated against the stopping criteria, which means to set the number of iterations or a generation limit. which then can be plotted as Pareto optimal solutions front from the designs can be selected and meta-models can be extracted [19], [26], [27].

B. Design variables

The inductor design is a very challenging multi-objective optimization problem. Aspects of this multi-objective optimization mentioned in this paper follow the process covered in [16]. To do this engineering decisions and certain range (design space ranges shown in Table III) have to be assigned. Similarly, constraints (or requirements), as shown in Table II, have to be determined and set up before executing the GA.

The ratios, rie, rec and rbe mentioned in the Table III, can be related directly to the dimensions mentioned in Fig. 4 (i.e. all aspects utilized for optimization can be directly translated into physical dimensions used to develop the model). The optimization algorithm considered 14 gene parameters. Fig. 6 directly translates all of the 14 gene parameters mentioned in Table III. The distribution of each of the ranges mentioned in the table is normalized and is shown in Fig. 6 to aid in understanding the impacts of the weightings of these parameters on the design. The blue colour indicates the initial parameter and the red colour indicated the convergence of each of the parameters (i.e. the best fit after many iterations).The material of the only conductor that is being considered is copper, due to cost, reliability, and other benefits. Litz wire is not being considered due to limited availability and high assembly overhead cost.

The loss calculation incorporates the DC conductor loss (I^2R), core loss and AC conductor loss. Core loss includes hysteresis loss density, (p_h), calculated by Modified Steinmetz

TABLE II
DESIGN SPECIFICATIONS FOR 2MH, 297A(RMS), 60HZ MMC INDUCTOR

Description	Value
Incremental Inductance	2mH
Maximum allowed current density	7.6 MA/m^2
Maximum allowed aspect ratio	3
Maximum allowed mass	200 kg
Maximum allowed loss	1 kW
Maximum allowed packing factor	0.7
Winding build factor	1.05
Minimum required magnetizing flux ratio	0.9
Maximum allowed Volume	0.1 m^3
No. of generation for GA	200
No. of population for GA	3000
No. of parallel strands of wire	10

TABLE III
INDUCTOR GA DESIGN SPACE

Min	Max	Gene	Symbols & Description	
1	8	1	Tcr	*Core material*
1	1	2	Tcd	*Conductor material*
1e^{-4}	0.1	3	g	*Air gap (m)*
0.1	10	4	lc	*Core length(m)*
1e-2	5	5	wc	*Center leg width(m)*
0.4	2	6	rec	*we to wc ratio*
0.4	3	7	rie	*wi to wc ratio*
0.4	3	8	rbe	*wb to wc ratio*
1e^{-4}	40	9	ac	*Conductor area (m^2)*
1	1e^3	10	N	*Desired number of turns*
1	7e^2	11	N_w	*slot width in conductors*
1	5e^2	12	N_d	*slot depth in conductors*
1e^{-6}	1e^{-1}	13	c_w	*Slot clearance in width (m)*
1e^{-6}	1e^{-1}	14	c_d	*Slot clearance in depth (m)*

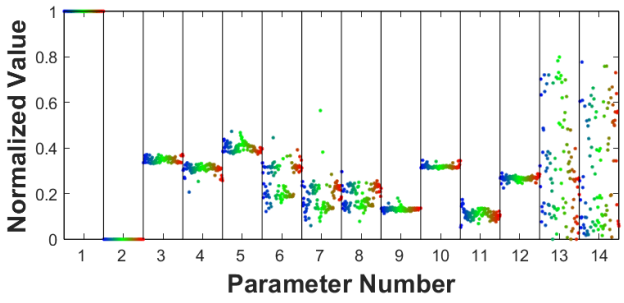

Fig. 6. Gene Distribution

978-1-7281-5672-9/20/$31.00 ©2020 IEEE

equation (MSE) and eddy current density, (p_e). AC conductor loss includes proximity loss and skin effect. The detailed explanation of modeling the multi-objective optimization using GA for mass, loss and volume is described in [16] and is also explained in Section V. Thermal analysis is not considered for this paper, but will be considered in future work.

V. Magnetic Losses of the Inductor

Magnetic losses in the inductor are divided into 3 different loss parameters: core losses, conductor losses and AC losses. Translation of the geometrical dimensions of the inductor core from the Figs. 3 and 4 into Magnetic equivalent Circuit (MEC) is established by dimensional flux analysis [28] and is used to determine incremental inductance.

A. Magnetic Core loss

Core loss in the inductor design for a medium voltage and high current will account for the major loss contribution. The loss calculation is divided into eddy current loss and hysteresis loss [29].

1) Eddy Current losses: Eddy currents in the magnetic material are induced by the time rate of change of flux, eddy current losses, and refer to the resistive losses associated with these induced currents. To evaluate the normalized power loss, flux density waveform is required and is calculated by

$$B = \frac{\mu_0 \mu_{\mathrm{r}} \mathrm{i}_{\mathrm{arm}}}{N w_c l_c} \tag{22}$$

where μ_0 is the permeability of free space and μ_r is the relative permeability of the material being used for the core. Also, to evaluate the system the time derivative of the system will be required given by

$$\frac{\mathrm{d}B}{\mathrm{d}x} = \frac{\mu_0 \mu_{\mathrm{r}}}{N w_c l_c} \frac{\mathrm{d}i_{arm}}{\mathrm{d}t} \tag{23}$$

and the volumetric power loss density is defined as

$$p_e = \frac{\sigma . w^2}{12} \frac{1}{T} \int_0^T \left(\frac{dB}{dt} \right)^2 dt \tag{24}$$

where p_e x volume of the core = total core loss due to eddy current.

2) Hysteresis Current losses: For accurate hysteresis loss calculation, the modified Steinmetz equation is used [30]. The equation for power loss density is given by

$$p_h = k_h \left(\frac{f_{eq}}{f_b} \right)^{\alpha - 1} \left(\frac{\Delta B}{2 B_b} \right)^{\beta} \tag{25}$$

where f_b and B_b are the base frequency and the base flux density f_{eq} is an equivalent frequency, defined by

$$f_{eq} = \frac{2}{\Delta B^2 \pi^2} \int_0^T \left(\frac{\mathrm{d}B}{\mathrm{d}x} \right)^2 dt \tag{26}$$

There are other variations of Steinmetz equation found in the literature for the interested reader [31], [32].

B. DC Conductor loss

DC conductor loss is clearly defined as the I^2R loss of the coil where R is the resistance of the coil and it is defined by

$$R = \frac{\mathrm{V_{cl}} \mathrm{N}^2}{\mathrm{k_{pf}} \mathrm{d_w^2} \mathrm{w_w^2} \sigma_{\mathrm{cd}}} \tag{27}$$

where k_{pf} is the packing factor and σ_{cd} is the conductivity of the selected copper.

C. AC conductor loss

AC conductor losses are concentrated towards the high end of the frequency spectrum and divide up into skin effect and proximity loss. The proximity effect, in this study, has much larger impact compared to the skin effect. One solution to the proximity effect challenge is to utilize multiple strands of parallel wire.

1) Skin effect in strip conductors: The skin effect in strip conductors is the tendency of AC current to distribute within the conductor such that the current density concentrates near the surface of the conductor and decreases with greater depths in the conductor for AC currents at the high end of the frequency spectrum. This consideration is extremely important to the consideration of utilizing simultaneously higher switching frequency and higher efficiency power semiconductors (such as Wide Band Gap) in order to reduce size, weight and cost of magnetic components. This frequency dependent current distribution leads to an uneven ohmic loss distribution in the conductor [33].

2) Proximity effect loss: The proximity effect is the tendency of the current to flow in other undesirable patterns (loops or concentrated distributions) due to the presence of magnetic fields generated by nearby conductors [34]. Proximity effect losses are defined as

$$P_P = D \overline{\left(\frac{di}{dt} \right)^2} \tag{28}$$

where D is the dynamic resistance it consists of

$$D = D_{ea} + D_{gcs} \tag{29}$$

$D_{ea}$is the dynamic resistance for the exterior adjacent and D_{gcs} is the dynamic resistance for the gaped closed slot.

VI. Optimization Results

Considering the specified core materials, Pareto optimal fronts for each of these materials were derived from the NSGA II based GA of the inductor according to the specifications of Table II, except for EPCOS N87. For this material, losses are above 3500W, for the specified inductor dimensions and, therefore, cannot be viewed in the same graph. The Pareto optimal fronts for mass versus loss and volume versus loss are shown in Figs. 7 and 8. Fig 7 shows volume versus magnetic loss, associated with the outside volume of the inductor core and coil assembly, for the range of core loss material variations. It should be noted that these volumes do not take into account the impacts of the dielectric insulation on the design (required for MVDC system application) but,

978-1-7281-5672-9/20/$31.00 ©2020 IEEE

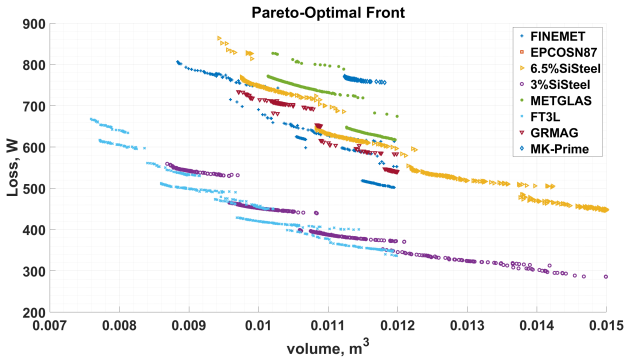

Fig. 7. Pareto-optimal front Volume vs loss

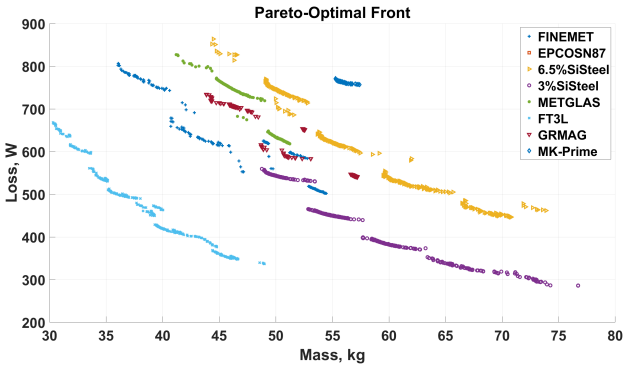

Fig. 8. Pareto-optimal front mass vs loss

instead, assume that the cabinet-level structure around the core and coil assembly will mitigate coil to core and coil to coil voltage stresses in order to meet requisite creepage, clearance and partial discharge withstand requirements. The impacts of these external mitigations on total system volume, as well as frame and structure mounting, are part of the overall system build-up [23], [35] and are not reflected in Fig 7. Trade-offs between voltage stress mitigations at the winding insulation level versus external stand-offs, and the impacts of field grading at points of connection to the inductor, will be addressed in future work.

Fig 8 shows inductor mass versus magnetic loss for the inductor for the range of core loss material variations. Comparing Fig. Fig 7 and 8 it is very interesting to note that the arm inductance loss and volume do not vary monotonically with total mass. This is due to various parameters that are being considered, but the major reason is the size of the radius of the conductor. The material FT3L results in lowest loss and volume. Cost is another factor to be considered in future studies.

The studies have converged closely to designs between 100 to 500 design executions. Mass of 200 kg and losses of 1kW are major limit to drive the designs in this sector and realizable design convergence. Completion of an optimization study takes $\sim$ 1 hours/run, hence it take $\sim$ 8 hours for all design runs on a Windows 10 i7-7700 2.8 GHz quad-core processor with installed RAM of 64GB. Validations using finite element methods and hardware implementation are not considered for this study and will be considered for future study.

VII. Conclusion

This work shows the formulation of anhystertic B-H characteristics and its corresponding permeability functions for the emerging new soft magnetic materials. Also comparative multi-objective optimized analysis of all these materials are analysed and the Pareto optimal fronts are presented. Multi-objective optimization was limited to mass,loss and volume. From this study the material FT3L has a clear advantage over other materials considered specifically in terms of lowest loss and lowest volume. The thermal analysis of these materials, i.e. construction of TEC and design of heat sync for this inductor is very crucial, therefore future studies are required to construct and test these significantly sized inductor.

Acknowledgement

The Authors would like to acknowledge Dr. Scott Sudhoff and Vinicius Nascimento from Purdue University for their ideas on the Inductor design.

References

[1] J. V. M. Farias, A. F. Cupertino, H. A. Pereira, S. I. Seleme, and R. Teodorescu, "On converter fault tolerance in mmc-hvdc systems: A comprehensive survey," *IEEE Journal of Emerging and Selected Topics in Power Electronics*, 2020.

[2] S. Debnath, J. Qin, B. Bahrani, M. Saeedifard, and P. Barbosa, "Operation, control, and applications of the modular multilevel converter: A review," *IEEE transactions on power electronics*, vol. 30, no. 1, pp. 37–53, 2014.

[3] R. A. J. Sahu, "Design Paradigm for Modular Multilevel Converter-Based Generator Rectifier Systems," *IEEE Open Access Journal of Power and Energy*, vol. 7, no. November 2019, pp. 130–140, 2020.

[4] Y. Li, E. A. Jones, and F. Wang, "Circulating current suppressing control's impact on arm inductance selection for modular multilevel converter," *IEEE Journal of Emerging and Selected Topics in Power Electronics*, vol. 5, no. 1, pp. 182–188, 2016.

[5] J. Gudex, M. Vygoder, R. Siddaiah, and R. M. Cuzner, "Recoverability of shipboard mvdc architectures," in *2020 IEEE Energy Conversion Congress and Exposition (ECCE)*. IEEE, 2020, pp. 6391–6398.

[6] W. Lin, D. Jovcic, S. Nguefeu, and H. Saad, "Protection of full bridge mmc dc grid employing mechanical dc circuit breakers," in *2017 IEEE Power & Energy Society General Meeting*. IEEE, 2017, pp. 1–5.

[7] T. Bandaru, T. Bhattacharya, and D. Chatterjee, "Minimization of the number of full-bridge submodules in hybrid modular multilevel converter," in *2018 IEEE International Conference on Power Electronics, Drives and Energy Systems (PEDES)*. IEEE, 2018, pp. 1–5.

[8] M. B. Ghat, A. Reddy, and A. Shukla, "Dc fault tolerant hybrid multilevel converter topologies for high power applications," in *2018 IEEE International Conference on Power Electronics, Drives and Energy Systems (PEDES)*. IEEE, 2018, pp. 1–6.

[9] N. Doerry, J. Amy, and C. Krolick, "History and the status of electric ship propulsion, integrated power systems, and future trends in the us navy," *Proceedings of the IEEE*, vol. 103, no. 12, pp. 2243–2251, 2015.

[10] L. Hong, Q. Xu, Z. He, F. Ma, A. Luo, and J. M. Guerrero, "Fault-tolerant oriented hierarchical control and configuration of modular multilevel converter for shipboard mvdc system," *IEEE Transactions on Industrial Informatics*, vol. 15, no. 8, pp. 4525–4535, 2018.

[11] R. M. Cuzner, R. Soman, M. M. Steurer, T. A. Toshon, and M. O. Faruque, "Approach to scalable model development for navy shipboard compatible modular multilevel converters," *IEEE Journal of Emerging and Selected Topics in Power Electronics*, vol. 5, no. 1, pp. 28–39, 2016.

978-1-7281-5672-9/20/$31.00 ©2020 IEEE

[12] R. Cuzner, S. Cruz, F. Ferrese, and R. Hosseini, "Power converter metamodeling approach for the smart ship design environment," in *2017 IEEE Electric Ship Technologies Symposium (ESTS)*. IEEE, 2017, pp. 118–125.

[13] R. Cuzner, R. Siddaiah, and T. Nguyen, "Applying a virtual prototyping process to generate pareto optimal solutions for a modular multi-level mvac to mvdc converter," in *2019 IEEE 28th International Symposium on Industrial Electronics (ISIE)*. IEEE, 2019, pp. 2039–2046.

[14] R. Siddaiah, "Derivation of power system module metamodels for early shipboard design explorations," 2019.

[15] G. M. Shane and S. D. Sudhoff, "Refinements in anhysteretic characterization and permeability modeling," *IEEE transactions on magnetics*, vol. 46, no. 11, pp. 3834–3843, 2010.

[16] S. D. Sudhoff, *Power magnetic devices: a multi-objective design approach*. John Wiley & Sons, 2014.

[17] N. E. T. Laboratory. TECHNICAL REPORTS SERIES (TRS). (2020, May 14). [Online]. Available: https://netl.doe.gov/TRS

[18] S. R. Moon, P. Ohodnicki, K. Byerly, and R. Beddingfield, "Soft magnetic materials characterization for power electronics applications and advanced data sheets," in *2019 IEEE Energy Conversion Congress and Exposition (ECCE)*. IEEE, 2019, pp. 6628–6633.

[19] S. D. Sudhoff and R. Sahu, "Metamodeling of rotating electric machinery," *IEEE Transactions on Energy Conversion*, vol. 33, no. 3, pp. 1058–1071, 2018.

[20] K. Deb, R. Hussein, P. C. Roy, and G. Toscano-Pulido, "A Taxonomy for Metamodeling Frameworks for Evolutionary Multiobjective Optimization," *IEEE Transactions on Evolutionary Computation*, vol. 23, no. 1, pp. 104–116, feb 2019.

[21] R. Cuzner, M. Vygoder, and R. Siddaiah, "Power Conversion and Distribution Equipment Metamodels for Dependable Design of Shipboard Integrated Power and Energy Systems," *2018 IEEE International Conference on Electrical Systems for Aircraft, Railway, Ship Propulsion and Road Vehicles and International Transportation Electrification Conference, ESARS-ITEC 2018*, pp. 1–8, 2019.

[22] R. Cuzner, R. Siddaiah, and T. Nguyen, "Applying a Virtual Prototyping Process to Generate Pareto Optimal Solutions for a Modular Multi-Level MVAC to MVDC Converter," *IEEE International Symposium on Industrial Electronics*, vol. 2019-June, pp. 2039–2046, 2019.

[23] R. Siddaiah, W. J. Koebel, and R. M. Cuzner, "Virtual prototyping of mv & hv modular multilevel power converter using evolutionary optimization based on ρ & η," in *2020 IEEE Energy Conversion Congress and Exposition (ECCE)*. IEEE, 2020, pp. 3532–3539.

[24] K. Deb, *Multi-objective optimization using evolutionary algorithms*. John Wiley & Sons, 2001, vol. 16.

[25] K. Deb, S. Agrawal, A. Pratap, and T. Meyarivan, "A fast elitist non-dominated sorting genetic algorithm for multi-objective optimization: Nsga-ii," in *International conference on parallel problem solving from nature*. Springer, 2000, pp. 849–858.

[26] R. Sahu and S. Sudhoff, "Design paradigm for modular multilevel converter based generator rectifier systems," Ph.D. dissertation, Purdue University Graduate School, 2019.

[27] H. Suryanarayana and S. D. Sudhoff, "Design paradigm for power electronics-based dc distribution systems," *IEEE Journal of Emerging and Selected Topics in Power Electronics*, vol. 5, no. 1, pp. 51–63, 2016.

[28] J. Cale, S. Sudhoff, and L.-Q. Tan, "Accurately modeling ei core inductors using a high-fidelity magnetic equivalent circuit approach," *IEEE Transactions on Magnetics*, vol. 42, no. 1, pp. 40–46, 2005.

[29] V. Karthikeyan, S. Rajasekar, S. Pragaspathy, and F. Blaabjerg, "Core loss estimation of magnetic links in dab converter operated in high-frequency non-sinusoidal flux waveforms," in *2018 IEEE International Conference on Power Electronics, Drives and Energy Systems (PEDES)*. IEEE, 2018, pp. 1–5.

[30] J. Reinert, A. Brockmeyer, and R. W. De Doncker, "Calculation of losses in ferro-and ferrimagnetic materials based on the modified steinmetz equation," *IEEE Transactions on Industry applications*, vol. 37, no. 4, pp. 1055–1061, 2001.

[31] J. Mühlethaler, J. Biela, J. W. Kolar, and A. Ecklebe, "Core losses under the DC bias condition based on steinmetz parameters," *IEEE Transactions on Power Electronics*, vol. 27, no. 2, pp. 953–963, 2012.

[32] ——, "Improved core-loss calculation for magnetic components employed in power electronic systems," *IEEE Transactions on Power Electronics*, vol. 27, no. 2, pp. 964–973, 2012.

[33] C. R. Sullivan, "Computationally efficient winding loss calculation with multiple windings, arbitrary waveforms, and two-dimensional or three-dimensional field geometry," *IEEE transactions on power electronics*, vol. 16, no. 1, pp. 142–150, 2001.

[34] X. Nan and C. R. Sullivan, "An improved calculation of proximity-effect loss in high-frequency windings of round conductors," in *IEEE 34th Annual Conference on Power Electronics Specialist, 2003. PESC'03.*, vol. 2. IEEE, 2003, pp. 853–860.

[35] R. Cuzner and R. Siddaiah, "Derivation of power system module metamodels for early shipboard design explorations," in *2019 IEEE Electric Ship Technologies Symposium (ESTS)*. IEEE, 2019, pp. 90–96.

978-1-7281-5672-9/20/$31.00 ©2020 IEEE